Report

Neuron

A Visual-Cue-Dependent Memory Circuit for Place Navigation

Highlights

- Fiber photometry allows for recording MEC-DG projection in freely moving mice
- A persistent-task-associated (PTA) activity is induced in the MECII-DG pathway
- PTA activity requires visual inputs throughout navigation to the learned place
- Photoinhibition of the MECII-DG activity causes a disruption of navigation

Authors

Han Qin, Ling Fu, Bo Hu, ..., Benedikt Zott, Arthur Konnerth, Xiaowei Chen

Correspondence

lfu@mail.hust.edu.cn (L.F.), arthur.konnerth@tum.de (A.K.), xiaowei_chen@tmmu.edu.cn (X.C.)

In Brief

Qin et al. identify a persistent-task-associated activity selectively in the medial entorhinal cortex layer II-hippocampal dentate gyrus pathway in freely moving mice after place learning. They find that this activity is required for navigation to the learned place.

Qin et al., 2018, Neuron *99*, 47–55
July 11, 2018
https://doi.org/10.1016/j.neuron.2018.05.021

CellPress

Neuron
Report

A Visual-Cue-Dependent Memory Circuit for Place Navigation

Han Qin,[1,2,7] Ling Fu,[2,7,*] Bo Hu,[3,7] Xiang Liao,[1] Jian Lu,[1] Wenjing He,[1] Shanshan Liang,[1] Kuan Zhang,[1] Ruijie Li,[1] Jiwei Yao,[1] Junan Yan,[1] Hao Chen,[3] Hongbo Jia,[4,5] Benedikt Zott,[5] Arthur Konnerth,[5,*] and Xiaowei Chen[1,6,8,*]
[1]Brain Research Center and State Key Laboratory of Trauma, Burns, and Combined Injury, Third Military Medical University, Chongqing 400038, China
[2]Britton Chance Center for Biomedical Photonics, Wuhan National Laboratory for Optoelectronics-Huazhong University of Science and Technology, Key Laboratory for Biomedical Photonics of Ministry of Education, School of Engineering Sciences, Huazhong University of Science and Technology, Wuhan 430074, China
[3]Department of Physiology, Third Military Medical University, Chongqing 400038, China
[4]Brain Research Instrument Innovation Center, Suzhou Institute of Biomedical Engineering and Technology, Chinese Academy of Sciences, Suzhou 215163, Jiangsu, China
[5]Institute of Neuroscience and the Munich Cluster for Systems Neurology, Technical University of Munich, 80802 Munich, Germany
[6]CAS Center for Excellence in Brain Science and Intelligence Technology, Chinese Academy of Sciences, Shanghai 200031, China
[7]These authors contributed equally
[8]Lead Contact
*Correspondence: lfu@mail.hust.edu.cn (L.F.), arthur.konnerth@tum.de (A.K.), xiaowei_chen@tmmu.edu.cn (X.C.)
https://doi.org/10.1016/j.neuron.2018.05.021

SUMMARY

The ability to remember and to navigate to safe places is necessary for survival. Place navigation is known to involve medial entorhinal cortex (MEC)-hippocampal connections. However, learning-dependent changes in neuronal activity in the distinct circuits remain unknown. Here, by using optic fiber photometry in freely behaving mice, we discovered the experience-dependent induction of a persistent-task-associated (PTA) activity. This PTA activity critically depends on learned visual cues and builds up selectively in the MEC layer II-dentate gyrus, but not in the MEC layer III-CA1 pathway, and its optogenetic suppression disrupts navigation to the target location. The findings suggest that the visual system, the MEC layer II, and the dentate gyrus are essential hubs of a memory circuit for visually guided navigation.

INTRODUCTION

The ability to navigate to known places with behaviorally relevant visual cues is fundamental to an animal's daily life and is often impaired in neuropsychiatric disorders like Alzheimer's disease (Albert, 2008). This cognitive function requires the formation of spatial memory to guide the navigation to desired locations in a familiar environment. Whereas theoretical and experimental evidence points to the entorhinal-hippocampal system as a key element in the neural networks for both spatial memory and navigation (Buzsáki and Moser, 2013; O'Keefe and Speakman, 1987; Steffenach et al., 2005), it is still largely unclear how this system contributes to the storage and representation of spatial information during navigation.

The entorhinal cortex extensively connects to neocortical areas and thus provides a major interface between sensory cortical areas and the hippocampus (Buzsáki and Moser, 2013; Moser et al., 2015). In particular, the medial entorhinal cortex (MEC) contains spatially modulated neurons (Hafting et al., 2005; Moser et al., 2015; Sargolini et al., 2006) and is thought to transmit spatial information to the hippocampus primarily through the trisynaptic pathway from MEC layer II (MECII) to dentate gyrus (DG) to CA3 to CA1 (van Strien et al., 2009; Zhang et al., 2013). Genetic manipulations or lesions of any of these elements in the pathway have revealed their critical roles in spatial learning and memory (Hales et al., 2014; Nakashiba et al., 2008, 2012; Nakazawa et al., 2002; Steffenach et al., 2005; Tennant et al., 2018; Yasuda and Mayford, 2006). In contrast, its parallel monosynaptic pathway from the MECIII to the CA1 appears less involved in spatial memory but is relevant for temporal association memory (Kitamura et al., 2015; Remondes and Schuman, 2004; Suh et al., 2011). However, despite this huge body of knowledge, whether and how these two MEC-hippocampal pathways generate representations of spatial cues and later use such stored information to search for specific places remained unclear.

Addressing these issues is challenging, largely owing to the difficulty of monitoring the real-time projection activity using standard electrophysiological or imaging methods while animals perform place-memory-related tasks. Here, we used axonal-projection-specific fiber photometry (Cui et al., 2013; Gunaydin et al., 2014) to track the activity of a group of MEC neuronal afferents projecting to the hippocampus in freely behaving mice. We used a Morris water maze (Morris et al., 1982) and an 8-arm radial maze (Eckerman et al., 1980), classic behavioral paradigms in which animals must remember and recall spatial information of landmarks to locate a hidden place over days of training. We found the *de novo* development of a place-learning-dependent activity pattern, which we term persistent-task-associated (PTA) activity, in the MECII-DG, but not the

MECIII-CA1 projection. Photoinhibition of the MECII-DG projection activity selectively abolished place memory, whereas inhibition of the MECIII-CA1 projection was ineffective. Our results suggest the MECII projection to the DG as an essential constituent of a memory circuit for place navigation.

RESULTS

Fiber-Photometry-Based Ca^{2+} Measurement in the MECII-DG Projection

For monitoring of the activity of axonal projections in freely behaving mice, we used an improved variant of optic fiber photometry (Cui et al., 2013; Gunaydin et al., 2014; Li et al., 2017). With this approach, it is possible to track neural activity in axon terminals expressing genetically encoded Ca^{2+} indicators (Figure 1A, top; Gunaydin et al., 2014). Here, the labeling of the MECII-DG projection with a Ca^{2+} indicator (Akerboom et al., 2012) was achieved by the targeted injection of an adeno-associated virus (AAV) carrying the GCaMP5G construct into the MECII (Figures 1A, bottom, S1A, and S1B). We verified that robust expression of GCaMP5G was restricted to the MECII (Figure 1B) and the corresponding projections to the DG (Figure 1C). This targeted injection led to only weak expression in the neighboring MECIII neurons (Figures 1B and S1C) and their projection axons in the stratum lacunosum moleculare (SLM) of the dorsal CA1 (Figure 1C, top). For MECII recordings, our analyses were restricted to those mice that had >80% (84.4% ± 2.4%) of GCaMP5G-labeled neurons in MECII. The overlay of viral expression areas across multiple mice confirmed the accuracy of the targeted expression in MECII (Figure S1D). For recording axonal activity, we implanted an optical fiber with the tip placed just above the MECII projection in the DG. This arrangement allowed for simultaneously exciting GCaMP5G and collecting its Ca^{2+}-dependent emission fluorescence (Figure 1A, bottom). The accurate position of fiber implantation was confirmed by post hoc histology (Figure S1E).

GCaMP5G-dependent Ca^{2+} recordings enabled the readout of the bulk activity of MECII-DG projections under both anesthesia and wakefulness (Figures S1F and S1G, blue; Video S1). Activity-dependent Ca^{2+} signals were not observed in control mice that expressed just EGFP (Figures S1F and S1G, purple). Stable Ca^{2+} recordings of the activity were reliably achieved over days. In 7 mice tested, the averaged amplitudes of the Ca^{2+} signals remained stable across an observation period of 2 weeks during open field exploration (Figures S1H and S1I). The local injection of muscimol, a $GABA_A$ (γ-aminobutyric acid)-receptor agonist, into the AAV injection site in the MECII completely blocked the projection Ca^{2+} signals in both anesthetized and freely behaving mice (Figures S2A, S2B, and S2D), indicating that the Ca^{2+} signals required neuronal firing and also that the observed transients were not caused or contaminated by motion artifacts (Figures S2C and S2D).

As visual cues were suggested to regulate hippocampal activity through connections between the visual and entorhinal cortices (Haggerty and Ji, 2015), we hypothesized that visual inputs would be the originating source of the activity in the MECII-DG projection during spatial exploration. Indeed, we observed that the intracranial crush of the optic nerves strongly reduced the projection signals during exploration (Figures S2E and S2F). By contrast, in the sham control group, the activity remained unchanged (Figure S2F). Control experiments confirmed that body movements minimally contributed to the fluorescence transients, as virtually no Ca^{2+} signals were detected in the MECII-DG projection during treadmill running, grooming, or eating (Figures S2G and S2H).

Place-Learning-Induced Development of PTA Activity in the MECII-DG Projection

To analyze the dynamics of MECII-DG projection during place navigation, we recorded the axonal activity in freely moving mice that were subjected to the Morris water maze (Figures 1D and 1E; Morris et al., 1982). After the end of 2^{nd} training day, the mice achieved a stable performance, with an averaged escape latency of <10 s (9.0 ± 0.9 s; range: 3.7–16.3 s; n = 10) to reach the hidden platform. Interestingly, the navigation-associated MECII-DG projection activity changed dramatically in an experience-dependent manner. Figure 1F shows recordings from a single example, whereas Figure 1G illustrates average trials from 6 mice. During the completely naive state (first trial on day 1), only small increases in Ca^{2+} activity were recorded during the initial exploratory navigation in the water pool (Figures 1F, 1G, left, S3A, and S3B). Instead, after the completion of two training days, on training day 3, the MECII-DG projection produced a larger and sustained Ca^{2+} signal, which we refer to as PTA activity (Figures 1F and 1G, right; Video S2). The Ca^{2+} level started at the beginning of the navigation and ended when the animal reached the hidden platform. Over repeated training sessions, the amplitude of the PTA activity gradually increased from an intermediate level, as observed during the 3^{rd} to 5^{th} training trials (Figures 1F and 1G, middle), to the final pattern that was highly characteristic for the well-trained state. The behavioral performance of the animals correlated tightly with the amplitude of the induced PTA activity (Figure 1H). The sustained phase of the Ca^{2+} signals, even the large ones in "expert" mice, was not due to dye saturation, as spontaneous, task not-related Ca^{2+} signals with even larger amplitudes were observed in the same mice during open field exploration (Figure S3C). Finally, we found that the duration of the PTA activity was a linear function of the escape latency throughout the learning process (Figure 1I), suggesting a direct role of the MECII-DG pathway for the animals' accurate navigation to the target place.

We next wondered about the activity status in the MECIII-CA1 pathway during navigation in the water maze. We used the same approach as that in the MECII to express GCaMP5G in the MECIII. We restricted our analyses to those mice that had the highest fractions of GCaMP5G-labeled neurons (98.3% ± 0.4%; see overlay of post hoc images from 6 animals in Figure S3D) in MECIII. Serial immunostaining images confirmed the selective expression of GCaMP5G in MECIII (Figures S3E–S3M). In contrast to our expectations (Buzsáki and Moser, 2013; Moser et al., 2015), we did not observe learning-dependent changes in neural activity of the projection over many trials of place learning. Unlike the observations in the MECII-DG projection, we observed a pronounced activity in the MECIII-CA1 projection already at the first trial at naive states, which, however, remained largely unchanged throughout the learning process (Figures 1J and 1K). In addition, we noted a slight increase in the level of Ca^{2+} activity while the animals were just

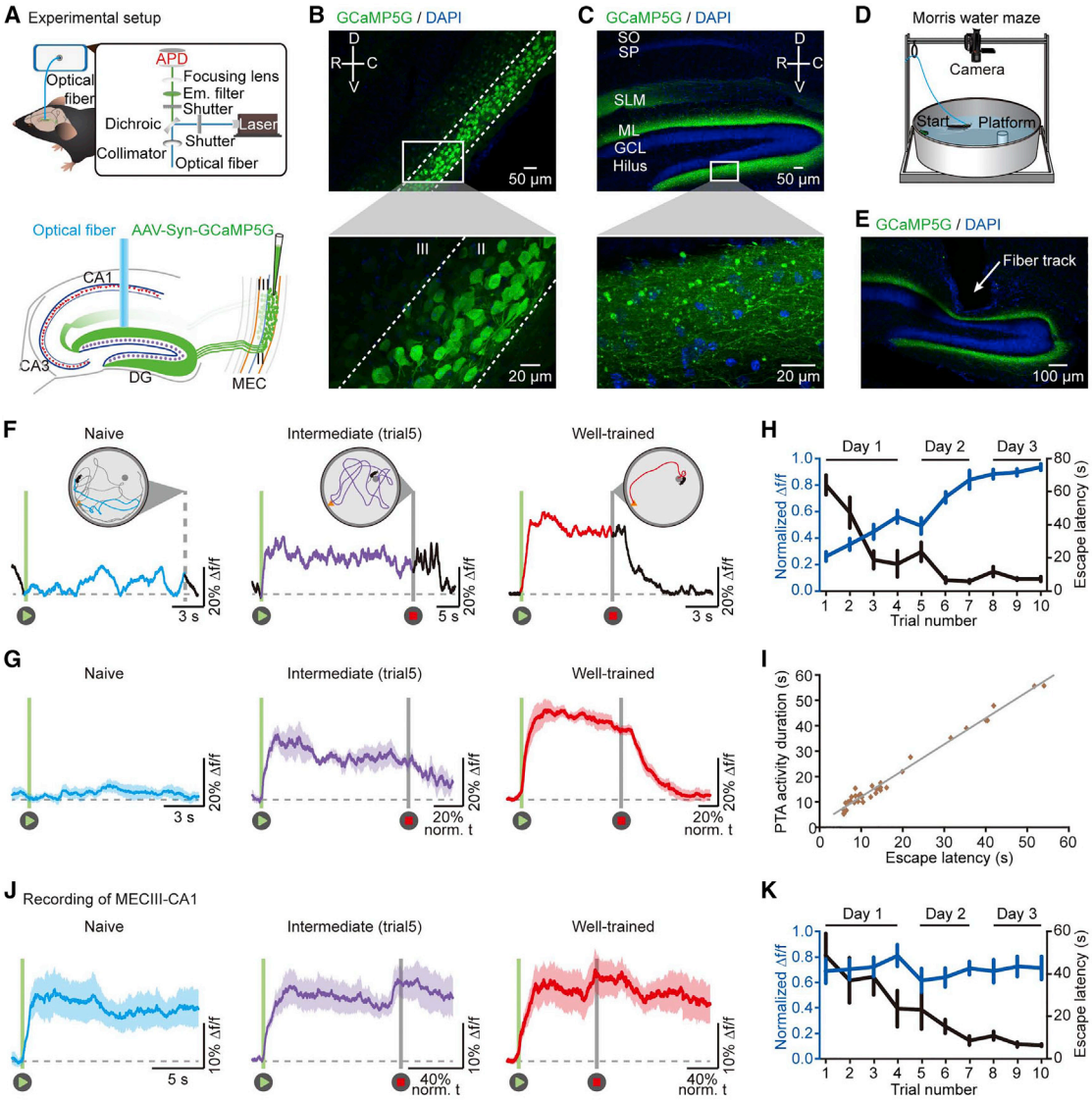

Figure 1. *De Novo* Induction of PTA Activity in the MECII-DG Projection over Place Learning

(A) Top: fiber photometry setup. APD, avalanche photo diode; Em., emission. Bottom: diagram shows viral injection and fiber recording.

(B and C) Confocal images showing GCaMP5G expression in the MEC (B) and the DG (C) from one mouse. The white rectangles (top) indicate the areas magnified at the bottom. C, caudal; D, dorsal; GCL, granule cell layer of DG; ML, stratum moleculare of DG; R, rostral; SLM, stratum lacunosum moleculare; SO, stratum oriens; SP, stratum pyramidale; SR, stratum radiatum; V, ventral.

(D) Schematic of the water maze.

(E) Histology after fiber recording as shown in (F). See also Figures S1 and S2.

(F) Example of the swim path (upper) and the corresponding Ca^{2+} signals (lower) in the MECII-DG projection at the naive (left), intermediate (middle), and well-trained (right) states. The Ca^{2+} signal traces and their corresponding swim paths are marked in blue, purple, or red. A green bar and a gray bar indicate the escape duration.

(G) Mean and SEM of Ca^{2+} signals from 6 mice. In the intermediate and trained states, the timescale was normalized to the corresponding escape latency.

(H) Plot of the amplitudes of Ca^{2+} signals (blue, Friedman rest; $p < 0.001$; $\chi^2 = 56.32$) and their corresponding escape latencies (black, Friedman rest; $p < 0.001$; $\chi^2 = 45.88$; $n = 8$ mice). Data are represented as mean ± SEM.

(I) Duration of PTA activity versus escape latency. The line indicates a linear fit ($R^2 = 0.98$; $n = 35$ trials).

(J) Mean and SEM of Ca^{2+} signals in the MECIII-CA1 projections from 7 mice.

(K) Plot of the amplitudes of Ca^{2+} signals (blue; Friedman test; $p = 0.64$; $\chi^2 = 35.76$) and their corresponding escape latencies (black; Friedman test; $p < 0.001$; $\chi^2 = 6.99$; $n = 7$ mice). Data are represented as mean ± SEM. See also Figure S3.

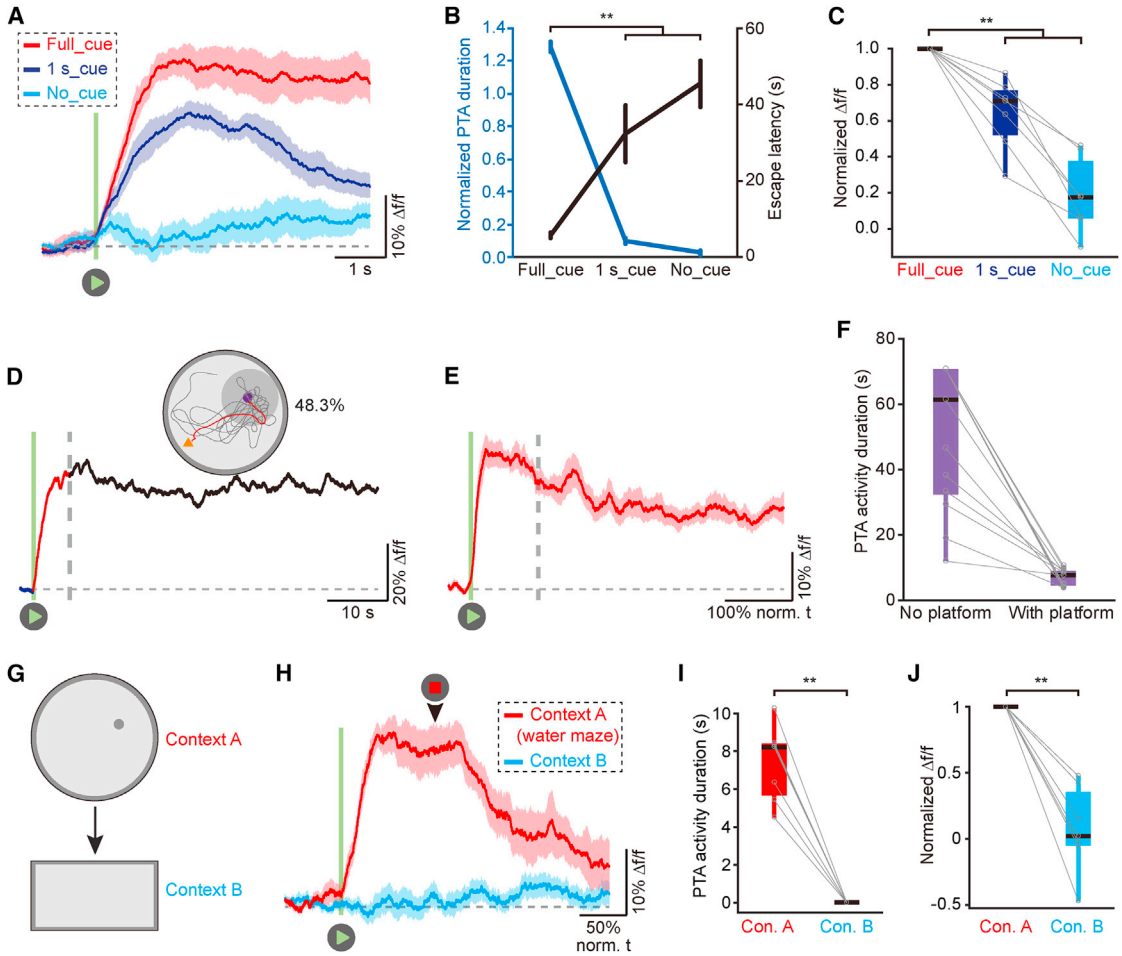

Figure 2. PTA Activity in the MECII-DG Projection Requires Continuous Visual Input in the Familiar Context

(A) Ca^{2+} signals in the MECII-DG projection during the conditions of full-cue, 1-s-cue, and no-cue presentations. The mean and SEM from 7 mice are shown. A green bar indicates the initiation of the task.

(B) Summary of the durations of PTA activity (blue; Wilcoxon signed-rank test; $^{**}p < 0.01$; $z = -2.28$) and their corresponding escape latencies (black; Wilcoxon signed-rank test; $^{**}p < 0.01$; $z = -2.28$; $n = 7$ mice). Data are represented as mean ± SEM.

(C) Summary of the amplitudes of Ca^{2+} signals. The amplitude was normalized to that in the full-cue condition. Wilcoxon signed-rank test; $^{**}p < 0.01$; $z = 2.28$; $n = 7$ mice.

(D) The prolongation of PTA activity in a trained mouse when the platform was removed. Inset, swim path. The gray area indicates the target quadrant. The first run from the start to the target position and the corresponding Ca^{2+} signals are marked in red.

(E) Mean and SEM from 6 mice.

(F) Comparison of the durations of PTA activity. Wilcoxon signed-rank test; $^{***}p < 0.001$; $z = 3.14$; $n = 13$ mice.

(G) Schematic of context A and context B.

(H) Ca^{2+} signals in the MECII-DG projection in context A (red) and context B (blue). Mean and SEM from 7 mice are shown. A green bar indicates the initiation of the task, whereas a black arrowhead indicates the end of task in context A. The timescale was normalized to the escape latency in context A.

(I) Summary of the durations of PTA activity. Wilcoxon signed-rank test; $^{**}p < 0.01$; $z = 2.28$; $n = 7$ mice.

(J) Summary of the amplitudes of Ca^{2+} signals. The amplitude was normalized to that in context A. Wilcoxon signed-rank test; $^{**}p < 0.01$; $z = 2.28$; $n = 7$ mice. Box-and-whisker plot, center line, median; box, 25%–75% interquartile range (IQR); whiskers, minimum and maximum.

touching the hidden platform. A similar destination-specific activity was observed in CA1 neurons in an annular water maze (Fyhn et al., 2002).

Visual-Input-Dependent Formation of PTA Activity in MECII-DG Projection

To further characterize the PTA activity, we performed several sets of experiments. First, we determined whether the PTA activity requires visual cue inputs throughout the navigation or only during the initial phase of the task. We used "no-cue" or "1-s-cue" trials, with the ambient light completely off or on just for 1 s following the onset of task, respectively, and compared them with initial, lights-on "full-cue" condition. As expected, in the no-cue condition, the mice were unable to navigate to the platform and the PTA activity was absent (Figures 2A–2C, light blue). In the 1-s-cue condition (Figures 2A–2C, blue), the mice

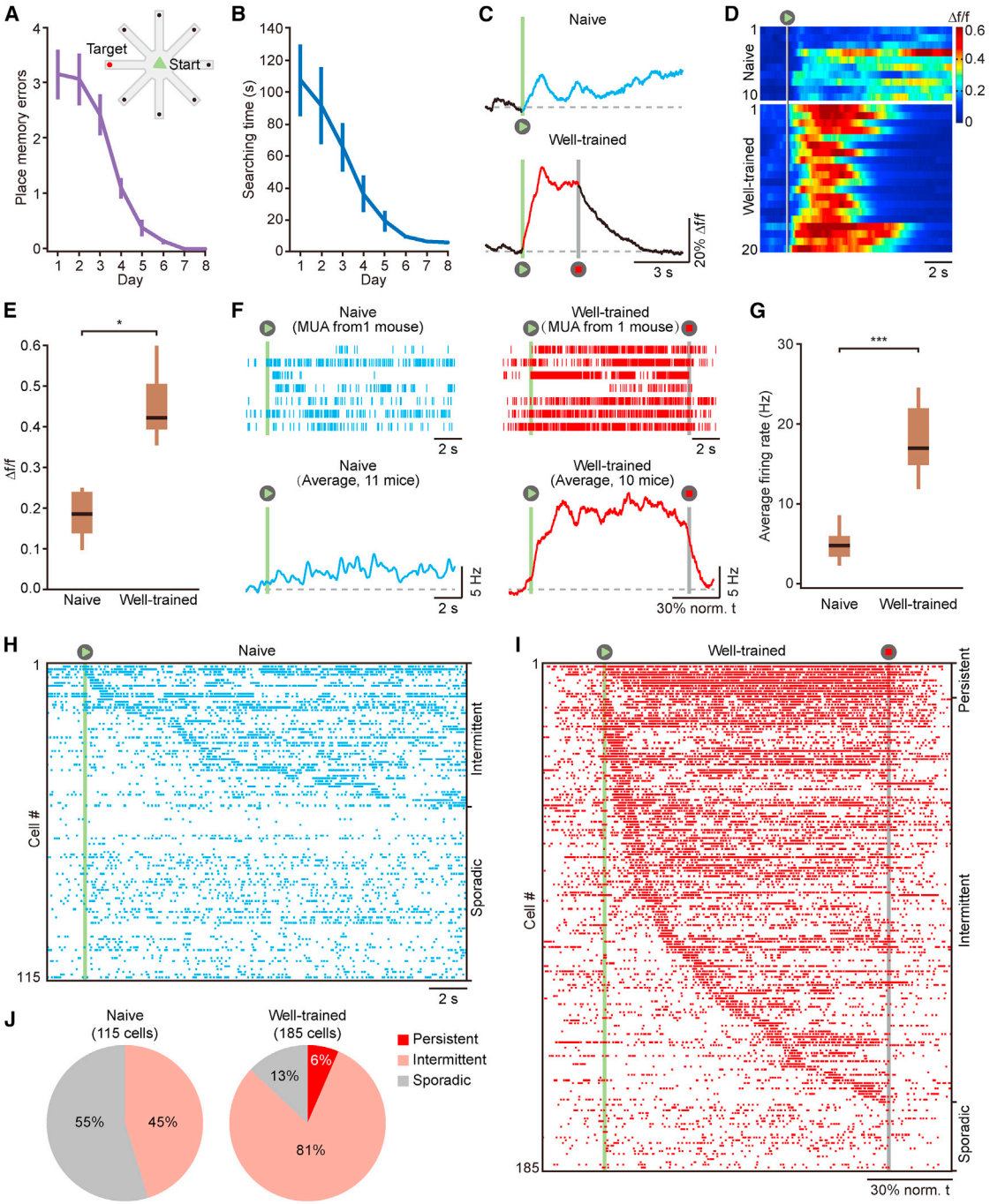

Figure 3. PTA Activity in the MECII-DG Projection in the Radial Maze and Electrophysiological Basis of the PTA Activity

(A and B) Summary of place memory errors (A; Friedman test; $p < 0.001$; $\chi^2 = 33.46$; $n = 5$; inset shows the radial arm maze setup) and searching time (B; Friedman test; $p < 0.001$; $\chi^2 = 33.07$; $n = 5$). Data are represented as mean ± SEM.

(C) Examples of Ca^{2+} signals from a mouse at naive (top) and well-trained states (bottom). The vertical green bars indicate the initiation of the task, and the vertical gray bar indicates the end of the task.

(D) Plot of amplitudes of Ca^{2+} signals of 10 naive trials (upper; two consecutive trials from each mouse) and 20 well-trained trials (lower; 4 consecutive trials from each mouse) from 5 mice.

(E) Comparison of the amplitudes of Ca^{2+} signals between naive and trained states (Wilcoxon signed-rank test; *$p < 0.05$; $z = -1.89$; $n = 5$).

(F) (Top) An example of MECII MUA from one mouse at its naive (left) and well-trained (right) states. (Bottom) The average firing rates from MECII MUA at naive (left; 11 mice) and well-trained (right; 10 mice) states are shown. At well-trained states, the timescale was normalized to the searching time.

(legend continued on next page)

initiated the navigation correctly but the navigation was prolonged and erratic (Figure 2B, black). Consistent with this deficit in behavior, the Ca^{2+} signals in the MECII-DG projection showed a normal initial rising phase, but the levels declined after the light was turned off (Figure 2A, blue). These results indicate that recall of memory during navigation is a dynamic process that requires sustained visual input until the animal reaches the hidden platform.

In a second set of experiments, we removed the platform. Compared to naive mice, well-trained mice showed a significant target quadrant preference (47.3% ± 3%; n = 10). Figure 2D illustrated an example of such recordings, in which we observed that the mouse navigated directly to the expected position of the platform with a latency <10 s (Figure 2D, red) and, after not finding the platform, continued its search. In line with the behavior, on average, the initial part of the PTA activity was unchanged but then persisted at a slightly decreased level in amplitude as the animal could not locate the platform (Figures 2E and 2F). Third, in well-trained mice, the PTA activity was completely absent when switching from the familiar water pool (context A) to a novel rectangular pool (context B; Figures 2G–2J). Together, these results suggest that the PTA activity, requiring continuous visual input and a task-dependent on-off pattern, encodes memory engrams that are essential for successful navigation to a learned place.

PTA Activity in the MECII-DG Projection in the 8-Arm Radial Maze

Next, we tested whether the PTA-like activity pattern was restricted to the water maze task. For this purpose, we used another type of place memory task, namely the 8-arm radial maze, and again recorded the activity of the MECII-DG projection (Figure 3A, inset). After a 6-day training, the mice were able to navigate to the target arm with no error trials and with a searching time of <10 s (7.2 ± 0.6 s; range 4.6–12.1 s; Figures 3A and 3B). We found no change in the running speed over training (9.2 ± 0.4 cm/s in naive versus 9.7 ± 0.5 cm/s in trained states; n = 15). We noted the buildup of a persistent activity that was similar to the PTA activity in the water maze (Figures 3C–3E), suggesting that the learned PTA activity in the MECII-DG projection is a general feature of place memories.

In order to determine the electrophysiological basis of the PTA Ca^{2+} signals, we used tetrode recordings to extracellularly monitor individual neurons in the MECII in the 8-arm radial maze. Our analyses were restricted to the recordings located between 5% and 30% of the dorsoventral extent of the MECII (Figure S4A; Table S1). We first analyzed multiunit activity (MUA) (Figures 3F and S4B) and found that the initial exploratory trials of naive mice were associated with a clear but rather modest increase in the level of activity in the MECII (Figure 3F, left). In contrast, on average, we found a persistent and strongly potentiated firing activity at the population level in well-trained mice (Figures 3F, right, and 3G). The learned increase in firing rate of MUA across all recordings exhibited a persistent pattern (Figure 3F, bottom in red) that matched well that of the Ca^{2+} activity in the projection, confirming their tight relationship.

Based on the analysis of single-unit activity (Figures 3H and 3I), we sorted all recorded MECII neurons into three classes, namely persistent, intermittent, and sporadic firing cells (see definition in STAR Methods). The persistent firing cells were completely absent in naive states but represented 6% of all recorded MECII neurons in well-trained states. By contrast, the fraction of intermittent firing cell increased from 45% in naive states to 81% in trained states (Figure 3J). Interestingly, in well-trained mice, 55% of the intermittent firing cells (82/149 cells) showed reliable firing activities at particular regions during navigation (Figures S4C and S4D), suggesting a spatially modulated activity pattern. Therefore, the PTA activity in the MECII-DG projection may be explained by the summation of the increase in the spike firing from a population of MECII neurons. This increase in population spike firing results from a development of persistent firing cells and a significant increment in the fraction of intermittent firing cells after place learning.

Impairment of Place Navigation by Photoinhibition of the MECII-DG Projection Activity

We used an optogenetic approach to test the causality between the experience-dependent PTA activity and successful navigation to the target. For this purpose, we bilaterally expressed the inhibitory opsin eNpHR3.0 in the MECII-DG projections (Gradinaru et al., 2010). To evaluate the effectiveness of eNpHR3.0 activation for the inhibition of the projection activity, we introduced a new variant of fiber photometry that enables simultaneous optogenetic inhibition and monitoring of Ca^{2+} activity in the same projections. The apparatus consists of a 488-nm-wavelength laser for exciting GCaMP5G, a 594-nm laser for activating eNpHR3.0, and a sensitive detector (a fast scientific complementary metal-oxide semiconductor [sCMOS] camera) for collecting the emission light (Figure 4A). We co-expressed GCaMP5G and eNpHR3.0 by confined viral injections to MECII neurons (Figures 4B and 4C). We found that light activation of eNpHR3.0 largely and reversibly reduced the amplitude of Ca^{2+} signals in the projection (Figures 4D, 4E, S4A, and S4B).

In the water maze, we used optic fibers that were bilaterally implanted above the corresponding MECII projection sites in the DG (Figure 4F). In 10/10 experiments performed in well-trained mice, optogenetic suppression of the projection activity disrupted their ability to directly navigate to the target (Figures 4G and 4H; Video S3). These mice had no abnormalities in swimming speed, eating, or open field exploration during light stimulation (Figures S4C–S4G). In the sham control group, 6 mice that expressed mCherry in the projection showed normal escape latencies with light stimulation (Figures 4G, bottom, and 4H, right). In addition, we subjected the mice to delayed fear conditioning, a hippocampus-independent associative learning task. We found that optogenetic silencing of the projection did not affect the fear levels 24 hr after conditioning (Figures S4H and S4I). Finally,

(G) The average firing rates from MUA (Wilcoxon rank-sum test; ***$p < 0.001$; $z = 3.84$; 11 mice for naive and 10 mice for trained states).
(H and I) Raster plot of single-unit activity from MECII neurons in naive (H) and trained (I) states.
(J) Pie charts showing the fractions of distinct cell classes in naive (115 cells; 11 mice) and well-trained (185 cells; 10 mice) states. See also Figure S4.
See also Table S1. Box-and-whisker plot: center line, median; box, 25%–75% IQR; whiskers, minimum and maximum.

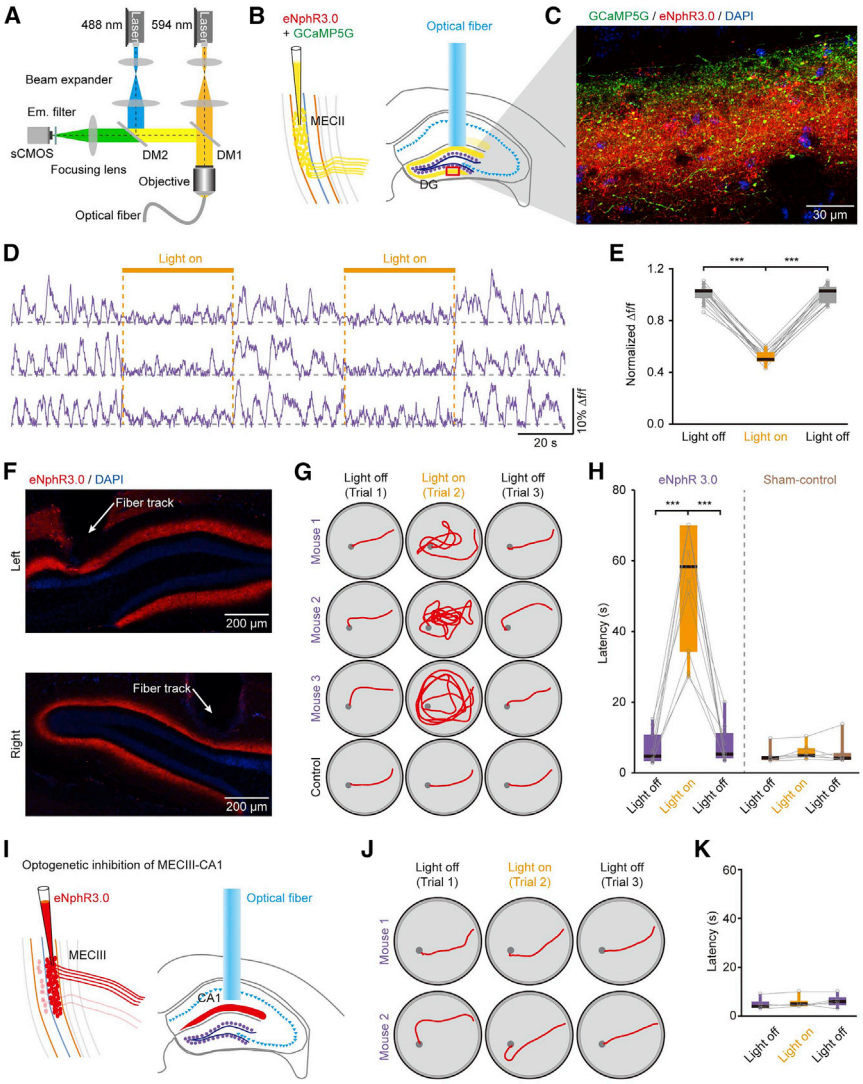

Figure 4. Photoinhibition of the MECII-DG Projection Activity Impairs Place Memory

(A) A new variant of fiber photometry device. DM, dichroic mirror.

(B) Diagram showing the co-expression of eNpHR3.0-mCherry and GCaMP5G in the MECII and fiber implantation above the DG.

(C) Confocal image showing the expression of GCaMP5G (green), eNpHR3.0 (red), and DAPI (blue) from a DG region.

(D) Example traces of Ca^{2+} signals in the MECII-DG projection with or without 594-nm light stimulation. Three anesthetized mice are shown.

(E) Summary of Ca^{2+} signals before, during, and after light stimulation. The amplitude of Ca^{2+} signals was normalized to the mean before light stimulation (Friedman test; ***$p < 0.001$; $\chi^2 = 24$; $n = 16$).

(F) Post hoc histology of eNpHR3.0 expression in both sides of the DG from a mouse.

(G) Examples of swim path in well-trained mice during consecutive light-off, light-on, and light-off trials. The first to third groups show three mice expressing eNpHR3.0. The last group shows one control mouse expressing mCherry.

(H) Summary of the effect of light-induced eNpHR3.0 activation on escape latency in the eNpHR3.0 (Friedman test; ***$p < 0.001$; $\chi^2 = 15.8$; $n = 10$) or control group (Friedman test; $p = 0.11$; $\chi^2 = 4.33$; $n = 6$).

(I) Diagram showing photoinhibition of the MECIII-CA1 projection.

(J) Examples of swim path in two well-trained mice expressing eNpHR3.0.

(K) Summary of the results from the MECIII-CA1 projection (Friedman test; $p = 0.21$; $\chi^2 = 3.11$; $n = 7$). See also Figure S5.

Box-and-whisker plot: center line, median; box, 25%–75% IQR; whiskers, minimum and maximum.

we bilaterally implanted optical fibers above the CA1 of the mice that expressed eNpHR3.0 in the MECIII-CA1 pathway (Figures 4I and S4J). Strikingly, photoinhibition of this pathway had no detectable effect on task performance in well-trained mice (Figures 4J and 4K). These optogenetic experiments reveal a unique and direct role of the MECII-DG activity in memory retrieval and place navigation.

DISCUSSION

How to find a known place includes two seemingly disparate processes, navigation and episodic memory (Buzsáki and Moser, 2013). It has been generally suggested that the MEC-hippocampal system has the anatomical and physiological properties that are suitable for processing both spatial navigation and memory. In particular, water maze experiments in which animals should learn spatial relations between landmarks to find a hidden position indicate that different subregions and pathways in this system are responsible for distinct aspects of place memory and navigation. For example, lesions or genetic manipulations of the MEC resulted in a significant deficit in place memory (Hales et al., 2014; Steffenach et al., 2005; Yasuda and Mayford, 2006). Lesions in the MECIII-CA1 pathway revealed its critical role for the consolidation of long-term place memory (4 weeks), but not for the acquisition and retrieval of short-term memory (24 hr; Remondes and Schuman, 2004). In the trisynaptic pathway, genetic manipulations have indicated that activity in the CA3 (Nakazawa et al., 2002) and CA3-CA1 transmission (Nakashiba et al., 2008) are involved in pattern completion, but not in the normal acquisition and retrieval of place memory with full-cue presentations. In addition, the DG granule cells were found to be required for both pattern completion and separation, but not for normal place memory function (McHugh et al., 2007; Nakashiba et al., 2012). However, despite extensive studies in this field, the dynamics of activity in the specific MEC-hippocampal pathways during place learning have not been recorded.

Here, we identified an experience-dependent pattern of activity, the PTA activity in the MECII-DG projection, the first stage of the MECII input into the hippocampus. As the DG, CA3, and CA3-CA1 pathway were suggested to be dispensable for the water maze version of place memory in the condition of full-cue presentations (McHugh et al., 2007; Nakashiba et al., 2008, 2012; Nakazawa et al., 2002), our work suggests that the MECII projection to the DG is a unique hub required for the storage of place memory in the entorhinal-hippocampal network. During navigation in the learned environment, this projection forms a representation of both the animal's instantaneous position and spatial information about the goal location through a sustained increase in population activity that the animal may use for efficient navigation.

Using electrophysiological recordings, we found a significant and persistent increase in the average firing activity at the population level of MECII neurons after place learning, which accounted for the persistent Ca^{2+} activity from a bundle of axonal fibers of MECII neurons. At the individual cell level, this summed increase in firing activity can be explained by two effects induced by place learning, namely the increase in the number of intermittent firing cells and the *de novo* induction of persistent firing cells. A large majority (81%) of MECII neurons was classified as intermittent firing cells in well-trained mice. Interestingly, ~55% of the intermittent firing cells exhibited spatially modulated activities at certain locations during navigation, suggesting that they may belong to the well-identified cell classes, including grid, border, head direction, or nongrid spatial cells (Diehl et al., 2017; Fyhn et al., 2004; Hafting et al., 2005).

As mentioned, a pause-free persistent firing pattern was observed in a small fraction (6%) of the recorded MECII neurons in trained mice. This pattern of activity was completely absent in naive mice and was reminiscent of persistent firing that has been previously described both *in vitro* and *in vivo* (Major and Tank, 2004). Persistent firing is thought to be related to different types of short-term memory (Fuster and Alexander, 1971; Romo et al., 1999) and is observed across different brain regions, including MECII/III and V (Egorov et al., 2002; Klink and Alonso, 1997; Yoshida et al., 2008). Earlier *in vivo* recordings have found persistent firing in the MEC during spatial working memory performance (Suzuki et al., 1997; Young et al., 1997). Additionally, MEC head direction cells display persistent firing when the animal's head is oriented in a particular direction (Taube and Bassett, 2003). It is also hypothesized that persistent firing in the MECIII may contribute to temporal associations (Kitamura et al., 2015; Suh et al., 2011; Yamamoto et al., 2014). Our results provide an *in vivo* experimental support for the existence of persistent firing in a small group of MECII neurons during navigation, although the exact mechanisms of its generation have yet to be experimentally investigated.

In conclusion, our findings extend previous knowledge on the various roles of the DG, CA3, and CA1 regions for place memory (McHugh et al., 2007; Nakashiba et al., 2008, 2012; Nakazawa et al., 2002) by identifying the MECII-DG projection as a specific memory circuit component for active place navigation. We suggest that the visual cue-dependent persistent activity of the MEC-hippocampal DG circuit encodes the mnemonic information needed for the successful navigation to learned places.

STAR★METHODS

Detailed methods are provided in the online version of this paper and include the following:

- KEY RESOURCES TABLE
- CONTACT FOR REAGENT AND RESOURCE SHARING
- EXPERIMENTAL MODEL AND SUBJECT DETAILS
  - Mice
- METHOD DETAILS
  - Virus Injection
  - Histology
  - Optical Fiber-Based Ca^{2+} Recording in Behaving Mice
  - Simultaneous Optical Fiber-Based Ca^{2+} Recording and Optogenetic Inhibition
  - Optogenetic Inhibition in Behaving Mice
  - Extracellular Electrophysiology in Behaving Mice
  - Water Maze
  - Radial Arm Maze
- QUANTIFICATION AND STATISTICAL ANALYSES
  - Data Analysis and Statistics

SUPPLEMENTAL INFORMATION

Supplemental Information includes five figures, one table, and three videos and can be found with this article online at https://doi.org/10.1016/j.neuron.2018.05.021.

ACKNOWLEDGMENTS

We thank Jia Lou for technical assistance, Dr. Wenjun Jin for assistance for experiments and data analyses, Dr. Liping Wang for viral vector production, and Dr. Sam McKenzie for his comments on the manuscript. This work was supported by the Nature Science Foundation of China (81671106, 61721092, 31700933, 61522502, and 81771175), "973Program" (2015CB759500), National Key Research and Development Program of China (2016YFA0201403 and 2017YFC0110002) and ULabor R&D Program (2017ULab0001), the Deutsche Forschungsgemeinschaft (SFB870), the Center for Integrated Protein Science Munich, and an Advanced Grant of the European Research Council to A.K. X.C. is a junior fellow of the CAS Center for Excellence in Brain Science and Intelligence Technology.

AUTHOR CONTRIBUTIONS

H.Q., L.F., A.K., and X.C. designed the experiments and wrote the paper. H.Q., L.F., B.H., J.L., W.H., K.Z., R.L., J. Yao, J. Yan, H.C., B.Z., and X.C. executed the experiments, analyzed the data, and completed the statistical analysis. X.L., S.L., and H.J. analyzed the data. H.Q., L.F., H.J., A.K., and X.C. designed and developed the recording devices. All authors read and commented on the manuscript.

DECLARATION OF INTERESTS

The authors declare no competing interests.

Received: December 11, 2017
Revised: April 3, 2018
Accepted: May 11, 2018
Published: June 14, 2018

REFERENCES

Akerboom, J., Chen, T.W., Wardill, T.J., Tian, L., Marvin, J.S., Mutlu, S., Calderón, N.C., Esposti, F., Borghuis, B.G., Sun, X.R., et al. (2012).

Optimization of a GCaMP calcium indicator for neural activity imaging. J. Neurosci. *32*, 13819–13840.

Albert, M. (2008). Neuropsychology of Alzheimer's disease. Handb. Clin. Neurol. *88*, 511–525.

Buzsáki, G., and Moser, E.I. (2013). Memory, navigation and theta rhythm in the hippocampal-entorhinal system. Nat. Neurosci. *16*, 130–138.

Cui, G., Jun, S.B., Jin, X., Pham, M.D., Vogel, S.S., Lovinger, D.M., and Costa, R.M. (2013). Concurrent activation of striatal direct and indirect pathways during action initiation. Nature *494*, 238–242.

Diehl, G.W., Hon, O.J., Leutgeb, S., and Leutgeb, J.K. (2017). Grid and nongrid cells in medial entorhinal cortex represent spatial location and environmental features with complementary coding schemes. Neuron *94*, 83–92.e6.

Eckerman, D.A., Gordon, W.A., Edwards, J.D., MacPhail, R.C., and Gage, M.I. (1980). Effects of scopolamine, pentobarbital, and amphetamine on radial arm maze performance in the rat. Pharmacol. Biochem. Behav. *12*, 595–602.

Egorov, A.V., Hamam, B.N., Fransén, E., Hasselmo, M.E., and Alonso, A.A. (2002). Graded persistent activity in entorhinal cortex neurons. Nature *420*, 173–178.

Fuster, J.M., and Alexander, G.E. (1971). Neuron activity related to short-term memory. Science *173*, 652–654.

Fyhn, M., Molden, S., Hollup, S., Moser, M.B., and Moser, E. (2002). Hippocampal neurons responding to first-time dislocation of a target object. Neuron *35*, 555–566.

Fyhn, M., Molden, S., Witter, M.P., Moser, E.I., and Moser, M.B. (2004). Spatial representation in the entorhinal cortex. Science *305*, 1258–1264.

Gradinaru, V., Zhang, F., Ramakrishnan, C., Mattis, J., Prakash, R., Diester, I., Goshen, I., Thompson, K.R., and Deisseroth, K. (2010). Molecular and cellular approaches for diversifying and extending optogenetics. Cell *141*, 154–165.

Gunaydin, L.A., Grosenick, L., Finkelstein, J.C., Kauvar, I.V., Fenno, L.E., Adhikari, A., Lammel, S., Mirzabekov, J.J., Airan, R.D., Zalocusky, K.A., et al. (2014). Natural neural projection dynamics underlying social behavior. Cell *157*, 1535–1551.

Hafting, T., Fyhn, M., Molden, S., Moser, M.B., and Moser, E.I. (2005). Microstructure of a spatial map in the entorhinal cortex. Nature *436*, 801–806.

Haggerty, D.C., and Ji, D. (2015). Activities of visual cortical and hippocampal neurons co-fluctuate in freely moving rats during spatial behavior. eLife *4*, e08902.

Hales, J.B., Schlesiger, M.I., Leutgeb, J.K., Squire, L.R., Leutgeb, S., and Clark, R.E. (2014). Medial entorhinal cortex lesions only partially disrupt hippocampal place cells and hippocampus-dependent place memory. Cell Rep. *9*, 893–901.

Hazan, L., Zugaro, M., and Buzsáki, G. (2006). Klusters, NeuroScope, NDManager: a free software suite for neurophysiological data processing and visualization. J. Neurosci. Methods *155*, 207–216.

Kitamura, T., Macdonald, C.J., and Tonegawa, S. (2015). Entorhinal-hippocampal neuronal circuits bridge temporally discontiguous events. Learn. Mem. *22*, 438–443.

Klink, R., and Alonso, A. (1997). Muscarinic modulation of the oscillatory and repetitive firing properties of entorhinal cortex layer II neurons. J. Neurophysiol. *77*, 1813–1828.

Li, J., Liao, X., Zhang, J., Wang, M., Yang, N., Zhang, J., Lv, G., Li, H., Lu, J., Ding, R., et al. (2017). Primary auditory cortex is required for anticipatory motor response. Cereb. Cortex *27*, 3254–3271.

Major, G., and Tank, D. (2004). Persistent neural activity: prevalence and mechanisms. Curr. Opin. Neurobiol. *14*, 675–684.

McHugh, T.J., Jones, M.W., Quinn, J.J., Balthasar, N., Coppari, R., Elmquist, J.K., Lowell, B.B., Fanselow, M.S., Wilson, M.A., and Tonegawa, S. (2007). Dentate gyrus NMDA receptors mediate rapid pattern separation in the hippocampal network. Science *317*, 94–99.

Meffert, M.K., Chang, J.M., Wiltgen, B.J., Fanselow, M.S., and Baltimore, D. (2003). NF-kappa B functions in synaptic signaling and behavior. Nat. Neurosci. *6*, 1072–1078.

Morris, R.G., Garrud, P., Rawlins, J.N., and O'Keefe, J. (1982). Place navigation impaired in rats with hippocampal lesions. Nature *297*, 681–683.

Moser, M.B., Rowland, D.C., and Moser, E.I. (2015). Place cells, grid cells, and memory. Cold Spring Harb. Perspect. Biol. *7*, a021808.

Nakashiba, T., Young, J.Z., McHugh, T.J., Buhl, D.L., and Tonegawa, S. (2008). Transgenic inhibition of synaptic transmission reveals role of CA3 output in hippocampal learning. Science *319*, 1260–1264.

Nakashiba, T., Cushman, J.D., Pelkey, K.A., Renaudineau, S., Buhl, D.L., McHugh, T.J., Rodriguez Barrera, V., Chittajallu, R., Iwamoto, K.S., McBain, C.J., et al. (2012). Young dentate granule cells mediate pattern separation, whereas old granule cells facilitate pattern completion. Cell *149*, 188–201.

Nakazawa, K., Quirk, M.C., Chitwood, R.A., Watanabe, M., Yeckel, M.F., Sun, L.D., Kato, A., Carr, C.A., Johnston, D., Wilson, M.A., and Tonegawa, S. (2002). Requirement for hippocampal CA3 NMDA receptors in associative memory recall. Science *297*, 211–218.

O'Keefe, J., and Speakman, A. (1987). Single unit activity in the rat hippocampus during a spatial memory task. Exp. Brain Res. *68*, 1–27.

Remondes, M., and Schuman, E.M. (2004). Role for a cortical input to hippocampal area CA1 in the consolidation of a long-term memory. Nature *431*, 699–703.

Romo, R., Brody, C.D., Hernández, A., and Lemus, L. (1999). Neuronal correlates of parametric working memory in the prefrontal cortex. Nature *399*, 470–473.

Roux, L., Hu, B., Eichler, R., Stark, E., and Buzsáki, G. (2017). Sharp wave ripples during learning stabilize the hippocampal spatial map. Nat. Neurosci. *20*, 845–853.

Sargolini, F., Fyhn, M., Hafting, T., McNaughton, B.L., Witter, M.P., Moser, M.B., and Moser, E.I. (2006). Conjunctive representation of position, direction, and velocity in entorhinal cortex. Science *312*, 758–762.

Schmitzer-Torbert, N., and Redish, A.D. (2004). Neuronal activity in the rodent dorsal striatum in sequential navigation: separation of spatial and reward responses on the multiple T task. J. Neurophysiol. *91*, 2259–2272.

Steffenach, H.A., Witter, M., Moser, M.B., and Moser, E.I. (2005). Spatial memory in the rat requires the dorsolateral band of the entorhinal cortex. Neuron *45*, 301–313.

Suh, J., Rivest, A.J., Nakashiba, T., Tominaga, T., and Tonegawa, S. (2011). Entorhinal cortex layer III input to the hippocampus is crucial for temporal association memory. Science *334*, 1415–1420.

Suzuki, W.A., Miller, E.K., and Desimone, R. (1997). Object and place memory in the macaque entorhinal cortex. J. Neurophysiol. *78*, 1062–1081.

Taube, J.S., and Bassett, J.P. (2003). Persistent neural activity in head direction cells. Cereb. Cortex *13*, 1162–1172.

Tennant, S.A., Fischer, L., Garden, D.L.F., Gerlei, K.Z., Martinez-Gonzalez, C., McClure, C., Wood, E.R., and Nolan, M.F. (2018). Stellate cells in the medial entorhinal cortex are required for spatial learning. Cell Rep. *22*, 1313–1324.

van Strien, N.M., Cappaert, N.L., and Witter, M.P. (2009). The anatomy of memory: an interactive overview of the parahippocampal-hippocampal network. Nat. Rev. Neurosci. *10*, 272–282.

Yamamoto, J., Suh, J., Takeuchi, D., and Tonegawa, S. (2014). Successful execution of working memory linked to synchronized high-frequency gamma oscillations. Cell *157*, 845–857.

Yasuda, M., and Mayford, M.R. (2006). CaMKII activation in the entorhinal cortex disrupts previously encoded spatial memory. Neuron *50*, 309–318.

Yoshida, M., Fransén, E., and Hasselmo, M.E. (2008). mGluR-dependent persistent firing in entorhinal cortex layer III neurons. Eur. J. Neurosci. *28*, 1116–1126.

Young, B.J., Otto, T., Fox, G.D., and Eichenbaum, H. (1997). Memory representation within the parahippocampal region. J. Neurosci. *17*, 5183–5195.

Zhang, S.J., Ye, J., Miao, C., Tsao, A., Cerniauskas, I., Ledergerber, D., Moser, M.B., and Moser, E.I. (2013). Optogenetic dissection of entorhinal-hippocampal functional connectivity. Science *340*, 1232627.

STAR★METHODS

KEY RESOURCES TABLE

REAGENT or RESOURCE	SOURCE	IDENTIFIER
Antibodies		
Rabbit anti-WFS1	Proteintech Group	Cat# 11558-1-AP; RRID: AB_2216046
Chicken anti-GFP	Abcam	Cat# ab13970; RRID: AB_300798
Alexa Fluor 488 donkey anti-chicken	Sigma- Aldrich	Cat# SAB4600031; RRID: AB_2721061
Alexa Fluor 568 donkey anti-rabbit	Invitrogen	Cat# A10042; RRID: AB_2534017
DAPI	Sigma-Aldrich	CAS: 28718-90-3
Bacterial and Virus Strains		
pAAV2/9-Syn-GCaMP5G	Obio Technology (Shanghai) Corp., Ltd.	N/A
pAAV2/9-Syn-GCaMP6f	Obio Technology (Shanghai) Corp., Ltd.	N/A
pAAV2/9-Syn-eGFP	Obio Technology (Shanghai) Corp., Ltd.	N/A
pAAV2/9-CaMKII-eNpHR3.0-mCherry	Shanghai Taitool Bioscience Corp., Ltd.	N/A
pAAV-CaMKII-mCherry	Obio Technology (Shanghai) Corp., Ltd.	N/A
Chemicals, Peptides, and Recombinant Proteins		
Muscimol hydrobromide	Sigma-Aldrich	CAS: 18174-72-6
Experimental Models: Organisms/Strains		
Mouse: C57BL/6J	Beijing HFK Bioscience Co., Ltd. (China)	https://www.jax.org/; JAX: 000664; RRID: IMSR_JAX:000664
Software and Algorithms		
MATLAB_R2016b	Mathworks	https://ww2.mathworks.cn/products/matlab.html; RRID: SCR_001622
LabVIEW 2014	National Instrument	http://www.ni.com/en-us/shop/labview/select-edition.html; RRID: SCR_014325
NeuroScope	Hazan et al., 2006	http://neurosuite.sourceforge.net
MClust	Schmitzer-Torbert and Redish, 2004	MClust
Recording software	Intan Technologies	Rhythm
Other		
Multimode optical fiber: MFP_200/230/900-0.48	Doric lenses	http://doriclenses.com/life-sciences/mono-fiber-optic/854-mono-fiber-optic-patch-cords-glass-048-053-na.html
488 nm solid-state laser: OBIS 488nm LX 50mW	Coherent	https://www.coherent.com/lasers/laser/cw-solid-state-lasers/obis-lasers/obis-lx-ls
Avalanche photodiode: S2382	Hamamatsu	http://www.hamamatsu.com/jp/en/product/category/3100/4003/4110/index.html
594 nm solid-state laser: MGL-F-593.5	Changchun New Industries	http://www.cnilaser.com/yellow_laser593.5.htm
RHD2000 USB interface board: C3100	Intan Technology	http://intantech.com/RHD2000_USB_interface_board.html
16 channel digital amplifier: C3334	Intan Technology	http://intantech.com/RHD2132_16channel_amp_board.html

CONTACT FOR REAGENT AND RESOURCE SHARING

Further information and requests for resources and reagents should be directed to and will be fulfilled by the Lead Contact, Dr. Xiaowei Chen (xiaowei_chen@tmmu.edu.cn)

EXPERIMENTAL MODEL AND SUBJECT DETAILS

Mice

Adult male mice C57BL/6J (2–3 months old at the initiation of the experimental procedure) were used for all of the recordings and behavior experiments. The mice were group housed, except for those implanted with optical fibers or electrodes. The animals had free access to food and water (except for those used for radial arm maze task) and lived under the condition of a 12 hr light/day cycle (lights on at 7:00 am). All the experimental procedures were performed in accordance with institutional animal welfare guidelines and were approved by the Third Military Medical University Animal Care and Use Committee.

METHOD DETAILS

Virus Injection

The mice were anesthetized with 1%–2% isoflurane in oxygen and then placed in a stereotactic head frame on a heating pad (37.5°C–38°C). After removing the skin, a small craniotomy (0.5 × 0.5 mm) was made above dorsal entorhinal cortex at −5.1 mm anteroposterior (AP) and 3.25 mm mediolateral (ML) from Bregma with a dental drill. A glass micropipette with a tip diameter of 10–20 μm (Figure S1A) was inserted to infuse the virus, starting at a depth of 1.6 mm dorsoventrally (DV, from the pial surface). Approximately 100 nL of virus solution was slowly injected while the pipette tip was gradually lifted until a depth of 1.2 mm DV (Figure S1B). Following the injection, the pipette was held in place for 2 min before retraction. The scalp incision was closed with tissue glue (3M Animal Care Products, Vetbond), and post-injection analgesics were provided for 3 days to help recovery.

We injected pAAV-Syn-GCaMP5G or pAAV-Syn-GCaMP6f for neuronal Ca^{2+} activity recording, pAAV-CaMKII-eNpHR3.0-mCherry for neuronal activity inhibition and pAAV-CaMKII-mCherry for control. The experiments were performed during the time window of ~4–10 weeks post-injection. When there were two viruses needed, the viral injections were carried out successively within a half-month interval.

Histology

To confirm the viral expression and the position of the optical fiber implantation, all of the animals were transcardially perfused with 4% paraformaldehyde (PFA) in PBS immediately following the experiments. After dehydration with 15% sucrose PBS for 24 hr, the brains were sectioned into 50 μm slices and stained with DAPI to visualize the nucleus. The images were acquired using a confocal microscope (Zeiss, LSM 700). For immunohistochemistry, the following primary antibodies were used: rabbit anti-WFS1 (1:200; Proteintech Group, 11558-1-AP), chicken anti-GFP (1:200; Abcam, ab13970). In addition, the following secondary antibodies were used: Alexa Fluor 488 donkey anti-chicken (1:200; Sigma, SAB4600031), Alexa Fluor 568 donkey anti-rabbit (1:500; Invitrogen, A10042).

Optical Fiber-Based Ca^{2+} Recording in Behaving Mice

A custom-built setup was used for neuronal Ca^{2+} signal measurements (Figure 1A) (Li et al., 2017). Optical fiber-based Ca^{2+} recording in the MECII-DG projection was performed as described previously (Figures S1D–S1H) (Gunaydin et al., 2014). Animals injected with pAAV-Syn-GCaMP5G in the MEC were anesthetized with 1%–2% isoflurane, and placed in a stereotactic head frame. A 200 μm diameter optical fiber (NA 0.48; Doric lenses, MFP_200/230/900-0.48) was glued into a short cannula (ID. 0.51 mm, OD. 0.82 mm) with the fiber tip extended approximately 2.5 mm out of the cannula. The preprocessed fiber was inserted through a small craniotomy made at the appropriate location (AP −2.2 mm, ML 2.0 mm) and advanced slowly toward the target position to near a depth of DV 1.8 mm for MECII-DG recording or 1.4 mm for MECIII-CA1 recording. Thereafter, the cannula was secured to the skull through a thin layer of UV-curing hardening dental cement (Tetric EvoCeram, 595953WW).

Neuronal Ca^{2+} signals and behavior videos were captured simultaneously during task performance. The Ca^{2+} signals were digitized at 2000 Hz with custom-written data acquisition software based on LabVIEW (National Instrument). The scene was illuminated with infrared light and the videos were recorded at 50 Hz with the spatial resolution of 1920 × 1080 pixels (Cannon, XA-25). All the Ca^{2+} signals and behavior videos were synchronized offline with event marks.

Simultaneous Optical Fiber-Based Ca^{2+} Recording and Optogenetic Inhibition

A new variant of optical setup was made to perform the simultaneous Ca^{2+} recording and the optogenetic inhibition through the same optical fiber (Figure 4A). GCaMP5G was excited by light from a solid-state laser (wavelength 488 nm, Coherent). The light intensity at the fiber tip was approximately 0.22 mW/mm^2. The emitted light was detected with an avalanche photodiode (Hamamatsu, S2382). The optogenetic inhibition protein eNpHR3.0 was activated by light from a solid-state laser (594 nm, Changchun New Industries). Optogenetic inhibition was conducted at 15 mW laser power in all of the experiments, and the light power at the fiber tip was 470 mW/mm^2. The laser control and the data acquisition were conducted using custom-written software in LabVIEW (National instrument).

Optogenetic Inhibition in Behaving Mice

The optical fiber implanted into the stratum molecular layer of dentate gyrus (SLM) was performed on both hemispheres as described above. The optogenetic inhibition light was turned off until the well-trained animal made a successful escape onto the platform and no

longer than 40 s of light was used in any of the behavioral experiments. The pulse duration and the power level were controlled by custom-written LabVIEW software. All of the optogenetic events were marked in the videos throughout the behavior tasks for offline analysis.

Extracellular Electrophysiology in Behaving Mice

For surgery, the animals were anesthetized with 1%–2% isoflurane, and then placed in a stereotactic head frame, with their eyes covered by ophthalmic ointment (Bepathen). The ground and reference screws were threaded into the bone above the cerebellum. A small craniotomy was made at the skull above the MEC (AP −5.1 mm, ML 3.12 mm) for the implantation of electrodes. Total of four tetrodes were assembled in a line array every 160 μm and mounted onto a home-made microdrive. A tetrode consists of four 25 μm insulated tungsten wires (California Fine Wire). The electrodes were inserted 1.2 mm below the cortical surface. After ~2–3 days recovery, the electrodes were gradually advanced to a final location of ~1.2–1.5 mm below the cortical surface. Throughout the training sessions in the radial arm maze, the electrophysiological signals were continuously acquired at 20 kHz on a RHD2000 USB interface board (Intan Technology, C3100), together with the video captured at 50 Hz under the spatial resolution of 1920 × 1080 pixels (Cannon, XA-25). All of the electrophysiological data and behavior videos were synchronized offline with event marks.

Water Maze

Place memory was assessed with an adapted procedure of the Morris water maze (Morris et al., 1982). In a circular swimming pool (120 cm in diameter, 40 cm high) containing water (20°C ± 1°C, made opaque by addition of titanium dioxide), the mice were trained to escape onto a hidden platform (10 cm in diameter, 10 cm high) that was 30 cm away from the pool wall and 1 cm below the water surface. The visual cues were placed onto the pool wall to support spatial references of the platform location. The platform location was fixed in all of the training trials. During each trial, the mice were released from the random starting positions and allowed to search for the platform for up to 70 s. The mice were allowed to stay for 20 s on the platform and then were placed back in the home cage during the 15-min interval time with the heater on. For partial cue experiments, well-trained mice were given a sequence test of "full-cue", "1 s-cue", "full-cue", "no-cue", and "full-cue" with an inter-trial interval of 15 min. The "full-cue" trial was the same as the training trial with illumination throughout the searching period. During the "1 s-cue" trial, the illumination was kept on for only 1 s immediately following the release of mouse into the pool. For the "no-cue" trial, no illumination was provided throughout the entire searching process. For testing the novel environment, we used a rectangle water pool setup that was completely different from the water maze pool in three features, including shape, color, and material. In addition, the new pool was placed in another environment with altered surrounding decorations. During all of the training and test trials, videos were recorded and the animal's locations were tracked using a custom-written MATLAB program.

Radial Arm Maze

A radial arm maze was also used to test place memory (Meffert et al., 2003). Eight arms radiated from the maze center (diameter 40 cm), with each arm being 50 × 10 cm in size. A small hole, which was invisible from the maze center, was made at the end of each arm to hold a small volume of water. Visual cues were placed surrounding the maze to support spatial references of the arms. The mice underwent water restriction with a half normal volume for two days before and throughout the training. During the training, a single arm was chosen to hold the water (0.1 mL), and the mice were released at the center of the maze to find the water's location. The maze task consisted of five trials per day across 8 days. We used in these tests only those animals with an 80% (80% ± 2%) time of locomotion activity during a 5-min exploration period.

QUANTIFICATION AND STATISTICAL ANALYSES

Data Analysis and Statistics

Fiber recording data were analyzed using the procedure similar to the previous work (Li et al., 2017). Briefly, all of the Ca^{2+} signals were collected at a sampling rate of 2000 Hz and were low-pass filtered by Savitzky-Golay FIR smoothing filter with 50 side points and a 3rd order polynomial. Relative fluorescence changes $\Delta f/f = (f - f_{baseline})/f_{baseline}$ were calculated as Ca^{2+} signals, where the $f_{baseline}$ was the baseline fluorescence taken during the entire recording period. To quantify the Ca^{2+} signals during the water maze test, the first frame when the animal was placed in the water was labeled as the start point. The earliest frame when the animal's whole body climbed onto the hidden platform was labeled as the end point, and the time between the start and the end point was counted as the escape latency. The duration of PTA activity was defined as the period in which Ca^{2+} signals were higher than 50% of the peak Δf/f.

For the electrophysiological recordings, the raw extracellular data were preprocessed to extract the spikes, as described previously (Roux et al., 2017). The constructed data were high-pass filtered (250 Hz) using a custom-written MATLAB program based on FFT spectrum analysis. All of the events that exceeded an amplitude threshold the four standard deviations above background were saved for subsequent spike sorting analysis. All of the detected events of each tetrode were initially classified into four clusters using a custom-written MATLAB program, with one cluster per wire. The clusters were sorted in a data visualization toolbox MClust (Schmitzer-Torbert and Redish, 2004) according to the waveform features. All of the events for each unit were visually examined within the raw traces using NeuroScope (Hazan et al., 2006). Interneurons were excluded based on narrower spike widths and higher firing rates (Fyhn et al., 2004).

For single unit activity analysis, the cell classification was performed according to the firing patterns. We calculated the firing rates of each cell in a sliding time window of 0.5 s (0.1 s interval) during the entire searching periods at well-trained states or during the first 20 s at naive states. Cells were defined as sporadic firing cells if the maximal firing rate was below the 75th percentile (i.e., 15 Hz) of the distribution of the average firing rate across all cells. Persistent firing cells were defined as the average firing rate was higher than 15 Hz and the minimal firing rate was above the 50th percentile (i.e., 7 Hz) of the distribution of the average firing rate across all cells. The remaining cells were defined as intermittent firing cells. Intermittent firing cells were classified into two groups, spatial and nonspatial cells. Cells were defined as spatial cells if they showed a stable spatially modulated firing activity pattern in at least two consecutive trials. In Figures 3H and 3I, intermittent firing cells were sorted in the order of the first peak time points of firing frequency.

All of the data were compared using non-parametric test. Four test methods were used throughout the work, including the Wilkinson signed-rank test for paired two-group analyses, the Wilkinson rank-sum test for unpaired two-group analyses, the Friedman test for paired multi-group analyses, and the Kruskal-Wallis test for unpaired multi-group analyses.